GWNet: A Lightweight Model for Low-Light Image Enhancement Using Gamma Correction and Wavelet Transform

Ming-Yu Kuo and Sheng-De Wang
Department of Electrical Engineering, National Taiwan University, Taipei, Taiwan
{*r11921053, sdwang*}*@ntu.edu.tw*

Keywords: Low-Light Image Enhancement, Light-Weighted Model, Gamma Correction, Wavelet Transform.

Abstract: Low-light image enhancement is essential for improving visual quality in various applications. We introduce GammaWaveletNet (GWNet), a novel approach that is composed of a gamma correction module and a wavelet network. The wavelet network is a sequential model with L subnetwork and H subnetwork. Both subnetworks use a U-Net architecture with Spatial Wavelet Interaction (SWI) component that is making use of wavelet transforms and convolution layers. The L subnetwork handles low-frequency components, while the H subnetwork refines high-frequency details, effectively combining spatial and frequency domain information for superior performance. Experimental results across datasets of different sizes demonstrate that GWNet achieves performance on par with state-of-the-art methods in terms of Peak Signal-to-Noise Ratio and Structural Similarity Index. Notably, the incorporation of wavelet transforms in GWNet leads to remarkable computational efficiency, reducing GFLOPs by approximately 75% and parameters by 40%, highlighting its potential for real-time applications on resource-constrained devices.

1 INTRODUCTION

Low-light image enhancement is a vital area of research within computer vision and image processing. Its importance is underscored by high-stakes applications such as surveillance, autonomous driving, medical imaging (Ullah et al., 2020), and photography. Images captured in such conditions often suffer from noise, low contrast, and detail loss, which can impair system performance and lead to significant risks in critical applications.

The primary challenges in this field stem from the computational complexity and the need for efficient algorithms. With increasing demand for lightweight models suitable for mobile and embedded devices, developing methods that optimize both performance and resource consumption is essential.

Conventional approaches (Wang et al., 2020b) such as gray-level transformation, histogram equalization (Banik et al., 2018), Retinex theory (Guo et al., 2016), and frequency domain methods aim to improve low-light images through direct image processing. However, these techniques often struggle with high computational costs, manual parameter tuning, and noise amplification.

Recent advancements in machine learning, especially Retinex-based models (Chen Wei, 2018; Zhang et al., 2022), enhance low-light images by refining illumination maps using histogram techniques. These methods address limitations of traditional approaches by leveraging the Retinex decomposition of reflectance and illumination components to improve visibility while maintaining color fidelity.

CNN-based models (Hussain et al., 2024; Wang and Zhang, 2024), utilizing advanced feature extraction, skip connections, and contextual aggregation, effectively mitigate noise and enhance contrast. Although they provide significant improvements, CNN-based models require extensive labeled datasets and high computational resources. Diffusion models (Jiang et al., 2023), though powerful in capturing global information and denoising, face challenges related to computational costs and detail preservation, limiting their practical deployment in resource-constrained environments.

Methods based on Fourier (Wang et al., 2023a; Huang et al., 2022) and wavelet transforms (Xu et al., 2022) apply frequency domain techniques to adjust image structure and brightness. While effective, these approaches can be computationally intensive and less adaptable to real-time applications.

We introduce "GammaWaveletNet (GWNet)", which integrates gamma correction, wavelet transforms, and CNN layers within a U-Net framework.

Kuo, M.-Y. and Wang, S.-D.
GWNet: A Lightweight Model for Low-Light Image Enhancement Using Gamma Correction and Wavelet Transform.
DOI: 10.5220/0013148800003890

In *Proceedings of the 17th International Conference on Agents and Artificial Intelligence (ICAART 2025) - Volume 2*, pages 264-274
ISBN: 978-989-758-737-5; ISSN: 2184-433X

This method aims to enhance image quality while reducing network complexity, outperforming traditional methods in both efficiency and performance.

Our contributions to low-light image enhancement are as follows:

- **Wavelet and Spatial Fusion.** Combining wavelet transforms with spatial domain data, our model preserves image details and minimizes artifacts.
- **Efficiency.** We reduce computational costs (FLOPs) and parameters, making the model suitable for deployment on devices with limited resources.
- **Scalability.** Our model demonstrates consistent performance across datasets of varying sizes, ensuring versatility in low-light image enhancement tasks.

2 RELATED WORK

In the related work section, we review gamma correction and wavelet-based enhancement methods, along with a Fourier-based model.

2.1 Gamma Correction

Gamma correction is a non-linear technique for adjusting image brightness. While it is widely used for brightness enhancement, selecting fitting parameters remains challenging, as improper gamma values can intensify noise in low-light regions and degrade image quality. To address this, several algorithms (Rahman et al., 2016; Cao et al., 2018) have been proposed for optimizing parameter selection.

The gamma correction formula (Huang et al., 2013) is given in Eq. 1, where I_{out} is the output image, I_{in} is the input image, and c and γ control the transformation curve:

$$I_{out} = c * I_{in}^{\gamma} \tag{1}$$

Traditionally, gamma correction is applied as a preprocessing step (Senthilkumar and Kamarasan, 2020). In contrast, our method integrates gamma correction into the training process, as done in (Wang et al., 2023b), allowing dynamic adjustment of luminance. This integration enables more precise and effective image enhancement during model training.

2.2 Wavelet Transform

The 2D Discrete Wavelet Transform (2D-DWT), illustrated in Fig. 1, decomposes an image of dimensions $M \times N$ into four subbands, each with dimensions $\frac{M}{2} \times \frac{N}{2}$. The Low-Low (LL) subband captures the image's average information, while the Low-High (LH), High-Low (HL), and High-High (HH) subbands capture horizontal, vertical, and diagonal details, respectively (Othman and Zeebaree, 2020). We refer to the LH, HL, and HH subbands as the high-frequency subbands, collectively denoted as YH. The wavelet transform is applied first along the rows and then along the columns, creating a hierarchical decomposition. In our work, we employ 2D-DWT (Ding, 2009; Mallat, 1999) with the Haar wavelet (Guf and Jiang, 1996), where H in Fig. 1 represents the Haar matrix, Eq. 2 represents the Haar matrix for a 1D signal of length 2, used for filtering operations.

$$H_0 = \frac{1}{\sqrt{2}}\begin{bmatrix}1 & 1\end{bmatrix}, \quad H_1 = \frac{1}{\sqrt{2}}\begin{bmatrix}1 & -1\end{bmatrix} \tag{2}$$

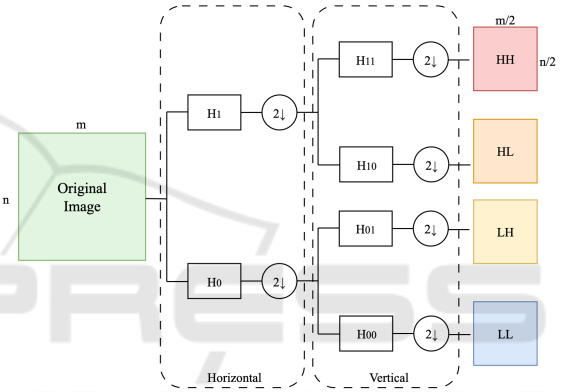

Figure 1: 2D Discrete Wavelet Transform Decomposition Tree (Weeks and Bayoumi, 2003): The wavelet transform divides the image into smaller frequency subband images, enabling more precise adjustments for different frequency features.

2.3 Fourier-Based Model

As noted in (Xu et al., 2021), the amplitude component in the Fourier domain represents an image's brightness, crucial for exposure correction, while the phase component captures structural details and is less affected by brightness changes. The Fourier transform-based low-light image recovery process uses the Fast Fourier Transform (FFT) to convert low-light and normal-light images into the frequency domain. By transferring the amplitude from the normal-light image to the low-light image and combining it with the phase of the low-light image, followed by an inverse FFT, effective relighting is achieved. FECNet (Huang et al., 2022) introduces a two-step process: an amplitude subnetwork enhances the low-light image's amplitude, which is then merged with the original low-light amplitude and processed through a phase subnetwork to refine image quality. In this study,

we further innovate by adapting the U-Net architecture within the Amplitude subnetwork, incorporating a spatial-frequency interaction block to better integrate spatial and frequency domain representations by using wavelet transform. This enhances FECNet's U-Net structure for improved integration between spatial and frequency images.

3 PROPOSED METHOD

This study introduces GammaWaveletNet (GWNet), a novel method combining gamma correction, wavelet transforms, and spatial image processing to enhance structural details and luminance in low-light images.

GWNet follows a sequential architecture for low-light image enhancement, as outlined in Fig. 2. Initially, gamma correction improves visibility in dark regions by adjusting luminance, with the gamma value estimated through CNN layers in Section 3.1. The GWNet has two subnetworks, as described in the following Section 3.2 to enhance the quality of the gamma correction enhanced image. In the L subnetwork then processes the image, enhancing low-frequency components via denoising and brightness adjustment. This output is passed to the H subnetwork, which refines high-frequency details by merging high-frequency components from the original low-light image with the enhanced low-frequency output in the shift block, as shown in Fig. 6. Both subnetworks employ a U-Net architecture, facilitating efficient feature extraction, denoising, and enhancement, resulting in clearer images across diverse lighting conditions.

Unlike traditional methods that only operate on wavelet sub-images (Ji and Jung, 2021), GWNet integrates spatial image data with wavelet-based networks, leveraging spatial and frequency domain information. This dual-domain approach effectively captures and enhances image features, leading to superior image quality.

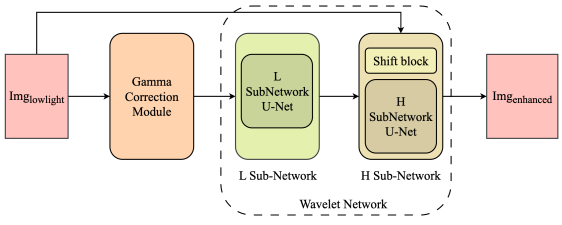

Figure 2: GWNet Model Structure: In GWNet, a sequential approach is used to enhance low-light images, and it is divided into gamma correction module and wavelet network.

3.1 Gamma Correction Module

Gamma correction is applied to adjust image brightness, enhancing visibility in dark regions and improving visual quality under poor lighting conditions. It modifies pixel intensity values to make dark areas more visible without oversaturating brighter regions.

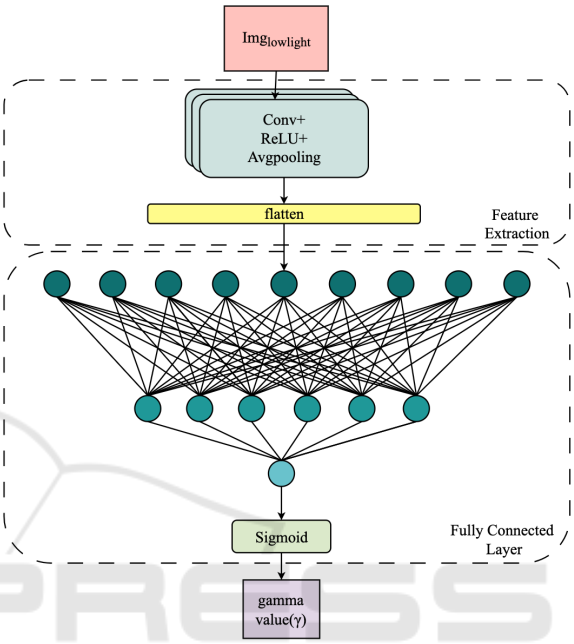

Figure 3: Gamma Correction Module: The gamma correction module utilizes feature extraction and fully connected layers to optimize image brightness enhancement.

We use a CNN structure, as illustrated in Fig. 3, to estimate gamma correction value (γ) for each image. This adjustment brings the image brightness to a suitable level, allowing subsequent wavelet network to further enhance and refine the image details. In standard CNN architectures (Sakib et al., 2019)(Bhatt et al., 2021), max pooling is often employed to select the maximum value within a pooling window, as defined in Eq. 3. Average pooling, defined in Eq. 4, computes the average value in a pooling window. In both equations, $x_{i,j}$ represents a 2D input, and pooling occurs over a window of size $k \times k$ (Yu et al., 2014). To improve stability and performance, we replace max pooling layers with average pooling.

$$\text{MaxPool}(x)_{i,j} = \max_{0 \le m < k} \max_{0 \le n < k} \{x_{i+m,j+n}\} \quad (3)$$

$$\text{AvgPool}(x)_{i,j} = \frac{1}{k^2} \sum_{m=0}^{k-1} \sum_{n=0}^{k-1} x_{i+m,j+n} \quad (4)$$

For low-light images, the CNN extracts features via convolutional layers, followed by ReLU activation

(Agarap, 2018) (Eq. 5) and average pooling. The extracted features are then processed through fully connected layers, with a sigmoid function constraining the predicted gamma value to an appropriate range. This gamma value is applied to the input image using Eq. 1, resulting in the output Img_{gamma}.

$$\text{ReLU}(x) = \begin{cases} x & \text{if } x \geq 0 \\ 0 & \text{if } x < 0 \end{cases} \quad (5)$$

3.2 Wavelet Network

In GWNet, two specialized subnetworks process different frequency components following wavelet decomposition: the Low-frequency (L) subnetwork in Section 3.2.1 and the High-frequency (H) subnetwork in Section 3.2.2.

The L subnetwork focuses on denoising and enhancing the brightness of the low-frequency components, specifically targeting the LL sub-image generated after gamma correction. This network effectively reduces noise and enhances clarity in low-frequency regions. The H subnetwork processes high-frequency components by combining the high-frequency details from the original low-light image with the output of the L subnetwork, preserving critical information such as edges and textures.

Both subnetworks employ a U-Net architecture, as shown in Fig. 4, inspired by (Huang et al., 2022). The U-Net's encoder-decoder framework (Ronneberger et al., 2015), along with the Spatial Wavelet Interaction (SWI) block in Section 3.2.3, facilitates feature extraction, denoising, and detail preservation, making it ideal for our method.

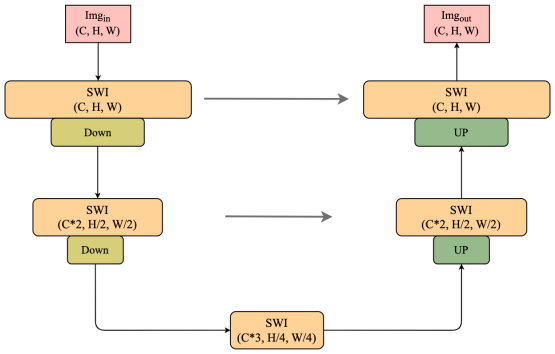

Figure 4: Wavelet subnetwork Structure: Both subnetworks use a U-Net architecture combined with the SWI block to enhance image quality.

In Fig. 4, C, H, and W represent the number of channels, height, and width of the feature maps. In the encoder path, downsampling layers capture increasingly abstract features. In the decoder path, upsampling reconstructs the image to its original resolution, with feature maps concatenated along the channel dimension with corresponding maps from the encoder.

3.2.1 L Subnetwork

The L subnetwork receives the gamma-corrected image Img_{gamma} as input, with the primary goals of denoising and enhancing brightness, particularly focusing on the low-frequency components in the LL sub-image.

As shown in Fig. 4, the L subnetwork is effective for image-to-image translation tasks. It denoises Img_{gamma} and continuously enhances brightness using a series of convolutional layers integrated with SWI blocks, as shown in Fig. 5. The SWI blocks in the L subnetwork specifically target the wavelet-transformed LL sub-image, which is essential for preserving the image's overall structure.

3.2.2 H Subnetwork

The H subnetwork processes the high-frequency subbands, specifically enhancing details and textures captured in the LH, HL, and HH sub-images of the wavelet transform. These components are essential for preserving image sharpness and fine details.

While similar to the L subnetwork, the H subnetwork incorporates a unique shift block utilizing the wavelet transform, as shown in Fig. 6. Although typically used for image relighting, the direct application of the shift function can hinder integration between low- and high-frequency sub-images. To address this, the output Img_{shift} is processed through a U-Net block (Fig. 4), which reduces noise in the high-frequency subbands and ensures better integration of the wavelet transform sub-images.

3.2.3 Spatial Wavelet Interaction (SWI)

The SWI block structure, shown in Fig. 5, is a crucial component in both the L and H subnetworks. It merges spatial and frequency domain information, improving input image quality. Though both subnetworks employ the SWI block, they have specific implementations to suit their respective tasks, as shown in Fig. 7 for frequency sub-images and spatial images. The spatial processing is consistent across both subnetworks, ensuring uniformity. The outputs from the SWI blocks are further processed to enhance image quality, focusing on brightness and denoising in the L subnetwork and texture refinement in the H subnetwork.

The SWI block processes and enhances the sub-images obtained from the wavelet transform by combining spatial features with frequency components.

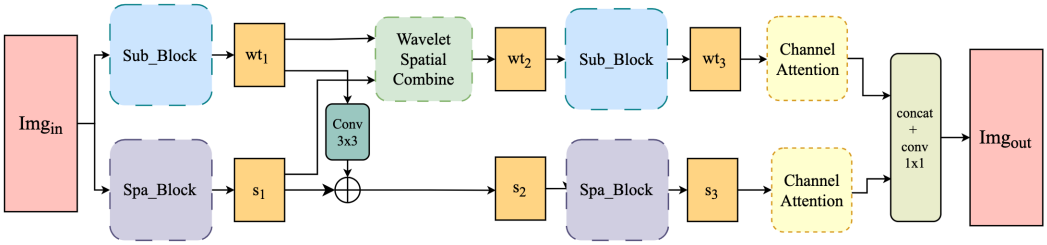

Figure 5: Spatial Wavelet Interaction Structure (SWI): Both subnetworks utilize SWI blocks to process different frequency subband images and the spatial image.

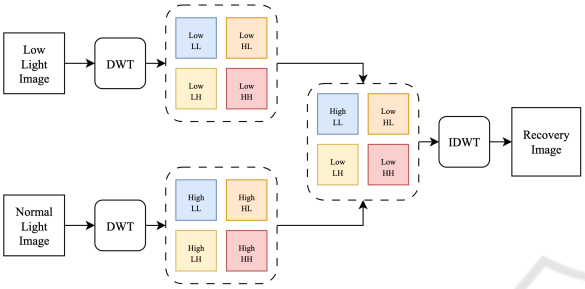

Figure 6: Wavelet Transform-Based Low-Light Image Recovery Process: This figure illustrates the wavelet transform-based recovery process, which serves as the shift block in our model.

This ensures comprehensive enhancement, with tailored handling of both low- and high-frequency details.

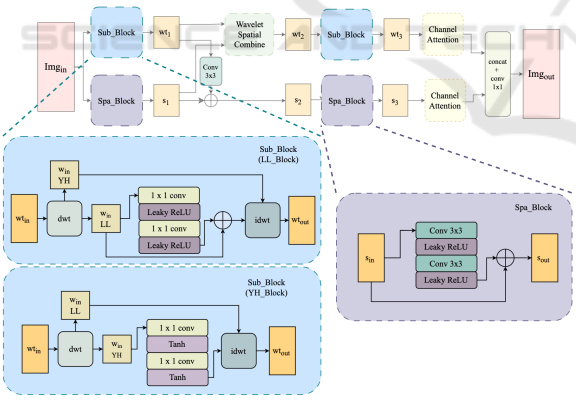

Figure 7: SWI Frequency Sub-Block for Different subnetworks and Spa-Block: The Frequency Sub-Block differs between the two subnetworks, tailored to low- or high-frequency subband images, while the Spa-Block processes spatial images.

In the L subnetwork, the SWI block processes the LL sub-image , which captures smooth, continuous features. The Leaky ReLU activation (Xu et al., 2015) is used to maintain structural information without harsh transitions, particularly useful for the LL subband.

In contrast, the SWI block in the H subnetwork handles the high-frequency subbands (LH, HL, HH), using the Tanh activation function (Mertens et al., 2004) to suppress noise while preserving fine details.

The SWI block combines the wavelet sub-image and spatial image, as illustrated in Fig. 8. After applying the Discrete Wavelet Transform (DWT) to both, the low-frequency subbands are enhanced using Leaky ReLU, and high-frequency subbands are processed with Tanh to reduce noise and enhance brightness. The final image is reconstructed using the Inverse DWT (IDWT).

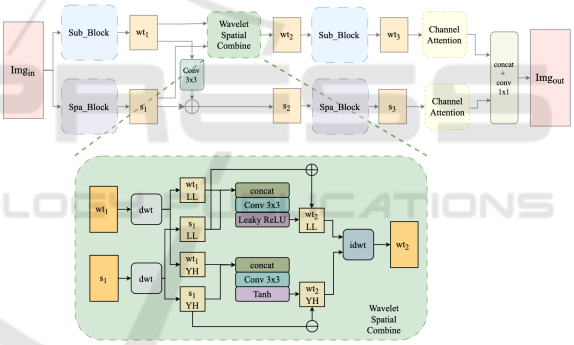

Figure 8: SWI Structure for Combining Frequency and Spatial Image: This block combines frequency and spatial images by utilizing wavelet subband images, tailored to different frequency characteristics.

The SWI block also includes a channel attention mechanism, shown in Fig. 5, inspired by Efficient Channel Attention (ECA) (Woo et al., 2018) and Convolutional Block Attention Module (CBAM) (Wang et al., 2020a). Both average and max pooling (Eq. 3 and Eq. 4) capture channel-wise statistics, followed by lightweight convolutional layers and sigmoid activation, improving feature selection for enhanced low-light image quality.

3.3 Loss Function

In our approach, we utilize multiple loss functions, including L1 loss, MSE loss (Janocha and Czarnecki,

2017), and SSIM loss (Nilsson and Akenine-Möller, 2020), to ensure effective training. Additionally, we incorporate the wavelet transform sub-images into the loss function to enhance the training process.

L1 loss (Eq. 6) calculates the average absolute differences between predicted and target values, while MSE loss (Eq. 7) estimates the mean squared error.

$$\text{L1 Loss} = \frac{1}{MN}\sum_{m=1}^{M}\sum_{n=1}^{N}|t_{m,n} - p_{m,n}| \tag{6}$$

$$\text{MSE Loss} = \frac{1}{MN}\sum_{m=1}^{M}\sum_{n=1}^{N}(t_{m,n} - p_{m,n})^2 \tag{7}$$

In these equations, t represents target images, and p represents predicted images, with dimensions $M \times N$.

SSIM loss measures the perceptual difference between the target and predicted images by considering structural information, luminance, and contrast. SSIM (Eq. 8) ranges from -1 to 1, and the SSIM loss is computed using Eq. 9. In Eq. 8, μ_t and μ_p represent the mean intensities, σ_t^2 and σ_p^2 indicate the variances, and σ_{tp} refers to the covariance. Constants c_1 and c_2 are included to stabilize the division process.

$$\text{SSIM}(t,p) = \frac{(2\mu_t\mu_p + c_1)(2\sigma_{tp} + c_2)}{(\mu_t^2 + \mu_p^2 + c_1)(\sigma_t^2 + \sigma_p^2 + c_2)} \tag{8}$$

$$\text{SSIM Loss} = 1 - SSIM(t,p) \tag{9}$$

Inspired by (Kim and Cho, 2023), we propose a loss function that leverages wavelet sub-images. Each subnetwork output is paired with a dedicated loss: the LL Loss in Algorithm 1 and the YH Loss in Algorithm 2. The LL Loss employs a combination of two loss functions on the low-frequency subband, ensuring both accurate reconstruction and enhancement of critical low-frequency features. In contrast, the YH Loss targets the high-frequency subbands. Since accurate reconstruction of small-scale features is essential, we use only the MSE loss, thereby simplifying the optimization process. Together, these loss functions effectively refine both low- and high-frequency subbands, preserving detailed information across multiple scales.

The total loss function is defined as:

$$\text{Total Loss} = \alpha \cdot \text{LL Loss} + \beta \cdot \text{YH Loss} + \delta \cdot \text{SSIM Loss} \tag{10}$$

where α, β, and δ are weights that balance the contribution of each loss term.

Input: L subnetwork output Img_{Lout}, target image $\text{Img}_{\text{target}}$
Output: LL Loss

Step 1: Apply 2D wavelet transform to obtain LL sub-images
$\text{LL}_{\text{Lout}} = \text{2D-DWT}(\text{Img}_{\text{Lout}})$
$\text{LL}_{\text{target}} = \text{2D-DWT}(\text{Img}_{\text{target}})$
Step 2: Calculate L1 and MSE Loss
$\text{L1 Loss} = \text{L1 Loss}(\text{LL}_{\text{Lout}}, \text{LL}_{\text{target}})$
$\text{MSE Loss} = \text{MSE Loss}(\text{LL}_{\text{Lout}}, \text{LL}_{\text{target}})$
Step 3: Combine Losses
$\text{LL Loss} = \text{L1 Loss} + \text{MSE Loss}$

Algorithm 1: LL Loss Calculation: The loss function for low-frequency subband image.

Input: H subnetwork output Img_{Hout}, target image $\text{Img}_{\text{target}}$
Output: YH Loss

Step 1: Apply 2D wavelet transform to obtain LH, HL, HH sub-images
$\text{LH}_{\text{target}}, \text{HL}_{\text{target}}, \text{HH}_{\text{target}} = \text{2D-DWT}(\text{Img}_{\text{target}})$
$\text{LH}_{\text{Hout}}, \text{HL}_{\text{Hout}}, \text{HH}_{\text{Hout}} = \text{2D-DWT}(\text{Img}_{\text{Hout}})$
Step 2: Calculate MSE Loss for each sub-image
$\text{MSE Loss}_{\text{LH}} = \text{MSE Loss}(\text{LH}_{\text{Hout}}, \text{LH}_{\text{target}})$
$\text{MSE Loss}_{\text{HL}} = \text{MSE Loss}(\text{HL}_{\text{Hout}}, \text{HL}_{\text{target}})$
$\text{MSE Loss}_{\text{HH}} = \text{MSE Loss}(\text{HH}_{\text{Hout}}, \text{HH}_{\text{target}})$
Step 3: Combine MSE Losses
$\text{YH Loss} = \text{MSE Loss}_{\text{LH}} + \text{MSE Loss}_{\text{HL}} + \text{MSE Loss}_{\text{HH}}$

Algorithm 2: YH Loss Calculation: The loss function for high-frequency subband image.

4 EXPERIMENTS

4.1 Datasets

In this research, we evaluate the performance of our method using two datasets of varying sizes, allowing us to demonstrate its effectiveness on both small and large datasets, as well as across diverse image resolutions.

The first dataset, LOL V1, designed for low-light image enhancement, contains 500 image pairs, 485 for training and 15 for testing, each with dimensions of 400x600 pixels. The dataset includes advanced post-processing to reduce artifacts caused by wind and hand movement, making it a reliable benchmark for algorithm evaluation, particularly in small-scale datasets. Initially introduced in (Chen Wei, 2018),

Table 1: Comparison of different approaches using various applied methods.

Method	RetinextNet (Chen Wei, 2018)	FourLLIE (Wang et al., 2023a)	FECNet (Huang et al., 2022)	WaveDiff (Jiang et al., 2023)	CDAN (Shakibania et al., 2023)	LYT-Net (Brateanu et al., 2024)	GWNet (Ours)
Retinex	✓	×	×	×	×	✓	✓
Frequency	×	✓	✓	✓	×	×	✓
Frequency-Spatial Interaction	×	×	✓	×	×	×	✓

Table 2: Quantitative results (PSNR, SSIM) on the each dataset: The best performance is marked in bold, while the second-best is marked in underlined.

Dataset	Metrics	RetinextNet (Chen Wei, 2018)	FourLLIE (Wang et al., 2023a)	FECNet (Huang et al., 2022)	WaveDiff (Jiang et al., 2023)	CDAN (Shakibania et al., 2023)	LYT-Net (Brateanu et al., 2024)	GWNet (Ours)
LoL-v1	PSNR	16.77	21.53	22.29	21.59	18.96	22.10	**22.33**
	SSIM	0.42	0.78	0.80	0.79	0.73	**0.82**	0.80
LSRW-Huawei	PSNR	16.82	21.09	**21.40**	20.10	19.73	20.62	21.36
	SSIM	0.38	0.62	0.61	0.51	0.54	0.61	**0.63**
LSRW-Nikon	PSNR	13.49	17.86	17.88	16.92	16.53	16.67	**17.90**
	SSIM	0.28	0.51	0.51	0.41	0.46	0.49	**0.52**

the LOL V1 Dataset serves as a critical benchmark for low-light enhancement methods.

The second dataset, LSRW Dataset, developed by (Hai et al., 2023), includes 5,650 image pairs: 3,170 captured with a Nikon D7500 and 2,480 with a Huawei P40 Pro. The images, sized at 960x640 for Nikon and 960x720 for Huawei, cover diverse indoor and outdoor scenes under low and normal-light conditions. Despite slight misalignments in some outdoor pairs, this dataset provides a comprehensive resource for evaluating low-light enhancement techniques, contributing to the robustness and generalizability of algorithms.

4.2 Results

To assess the effectiveness of various methods, we employ the following metrics: Peak Signal-to-Noise Ratio (PSNR)(Horé and Ziou, 2010), Structural Similarity Index (SSIM)(Wang et al., 2004), parameter count (Params), and Floating Point Operations (FLOPs).

4.2.1 Comparative Analysis with Existing Methods

Our experiments compare the proposed GWNet method with several advanced techniques, including the Retinex method (Chen Wei, 2018), Fourier-based methods (Wang et al., 2023a; Huang et al., 2022), and Diffusion models (Jiang et al., 2023). We also evaluate the impact of post-processing (Shakibania et al., 2023) and different data formats (Brateanu et al., 2024) on performance. Table 1 presents a comparison of these advanced approaches, utilizing various methods for low-light image enhancement, including Retinex, frequency-based techniques, and combined frequency and spatial interactions. Our proposed method incorporates all of these approaches.

4.2.2 Quantitative Results Compare with Existing Methods

The comparisons are conducted using two datasets: LOL V1 and LSRW. The LSRW dataset is further divided into two subsets, Huawei and Nikon, based on the cameras used for capturing the images.

GWNet has demonstrated exceptional performance across these datasets, surpassing other state-of-the-art methods, as shown in Table 2. This confirms GWNet's effectiveness and versatility in low-light image enhancement tasks. On the LOL V1 dataset, GWNet achieves the highest PSNR of 22.33 dB and a competitive SSIM of 0.80, indicating its ability to enhance image quality while preserving structural details. In the LSRW_Huawei subset, GWNet shows strong performance with a PSNR of 21.36 dB and the highest SSIM of 0.63, reflecting superior detail preservation and perceptual quality. Similarly, in the LSRW_Nikon subset, GWNet achieves a PSNR of 17.90 dB and an SSIM of 0.52, demonstrating its robustness across various imaging conditions.

Fig. 9, 10, and 11 show example results from the LOL V1, LSRW_Huawei, and LSRW_Nikon datasets, respectively. Each figure presents a sample image demonstrating the performance of different models. These examples illustrate that GWNet consistently delivers balanced results under various low-light conditions. The red boxes highlight zoomed-in areas for closer examination of image quality, showcasing the enhancement of specific details. GWNet excels in improving image quality, reducing noise, and preserving structural details across all datasets, making it a robust solution for low-light image enhancement.

4.2.3 Computational Efficiency Compare with Existing Methods

One of the key strengths of GWNet is its exceptional computational efficiency, as demonstrated in Table 3. With only 0.027 M parameters and 0.89 GFLOPs,

Table 3: Model Complexity Comparison: The best performance is marked in bold, while the second-best is marked in underlined.

Method	RetinextNet (Chen Wei, 2018)	FourLLIE (Wang et al., 2023a)	FECNet (Huang et al., 2022)	WaveDiff (Jiang et al., 2023)	CDAN (Shakibania et al., 2023)	LYT-Net (Brateanu et al., 2024)	GWNet (Ours)
Params(M)	0.84	0.12	0.15	22	3.5	<u>0.045</u>	**0.027**
FLOPs(G)	587.47	5.83	13.24	197.89	5.07	<u>3.49</u>	**0.89**

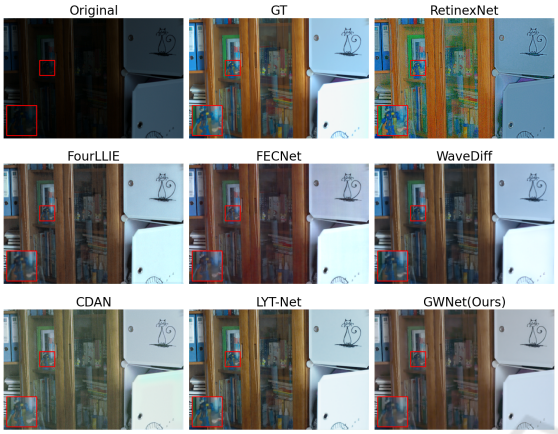

Figure 9: LOL V1 Result: A comparison of one example produced by each model, alongside the low-light image and the ground truth from the LOL V1 dataset.

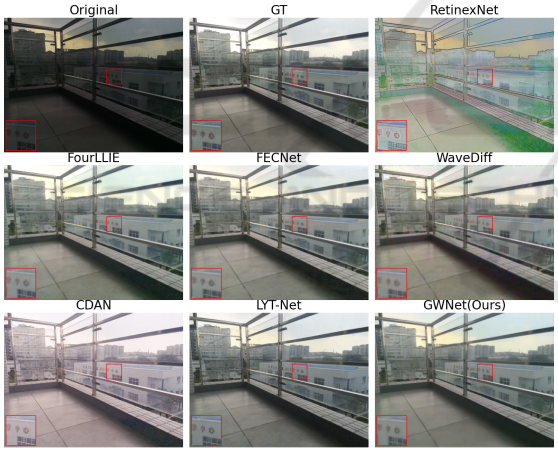

Figure 10: LSRW_Huawei Result: A comparison of one example produced by each model, alongside the low-light image and the ground truth from the LSRW_Huawei dataset.

GWNet reduces GFLOPs by approximately 75% and parameters by 40% compared to other methods. This makes GWNet the most lightweight model among those compared, making it ideal for real-time applications on resource-constrained devices such as portable phones and embedded systems.

4.2.4 Ablation Study

In our ablation experiment, we compare different structural configurations of our model using the LOL V1 dataset. First, we assess the impact of applying a single gamma correction value across the entire dataset versus assigning a unique value to each image. Second, we investigate the effect of using leaky ReLU in the L subnetwork for processing low-frequency sub-images, similar to the spatial image. These configurations are evaluated using PSNR and SSIM metrics, and the observed differences are discussed.

Figure 11: LSRW_Nikon Result: A comparison of one example produced by each model, alongside the low-light image and the ground truth from the LSRW_Nikon dataset.

Table 4 presents the results of the LOL V1 dataset comparison, exploring different gamma correction methods and activation functions for low-frequency sub-image processing. Since each image in the dataset contains multiple light sources, assigning a single gamma value across the dataset (`gamma_dataset`) fails to address the variations in light intensity. Conversely, assigning a unique gamma correction value for each image (`gamma_image`) provides more accurate corrections, leading to improved enhancement results. For the low-frequency (LL) sub-image, which captures the overall structure of the image, we find that using leaky ReLU (`leakyReLU_L`) helps maintain structural integrity. Unlike high-frequency components that benefit from the tanh activation function (`tanh_L`), the LL sub-image requires leaky ReLU to avoid limiting the range, ensuring better preservation of structural details.

The ablation study reveals that using unique gamma correction values for each image (`gamma_image`) and leaky ReLU for LL sub-images results in improved PSNR. However, the SSIM for

Table 4: Ablation study on LOL V1 dataset: The best performance is marked in red and bold, while the second-best is marked in blue and underlined.

Configuration	PSNR	SSIM
gamma_dataset + tanh_L	19.24	0.77
gamma_dataset + leakyReLU_L	<u>21.79</u>	**0.82**
gamma_image + leakyReLU_L	**22.33**	<u>0.80</u>

this configuration is slightly lower than when using a single gamma value with leaky ReLU. This slight decrease in SSIM may be attributed to the increased complexity and variability introduced by the different gamma values.

We performed an error map analysis to evaluate the impact of each subnetwork on overall enhancement quality. As illustrated in Fig. 12, two example images from the LOL V1 dataset highlight the differences between the ground truth and the outputs from various stages of our model. These visualizations provide insight into the contributions of the L and H subnetworks in reducing errors and enhancing image quality.

The visualizations include a low-light image, a normal light image (ground truth), and the outputs Img_{Lout} and Img_{Hout}, representing the results from the L subnetwork and H subnetwork, respectively. The error maps reveal how the L subnetwork significantly improves the low-light image, while further processing Img_{Lout} through the H subnetwork leads to Img_{Hout}, showing even greater enhancement. This two-stage process effectively reduces noise and improves image quality.

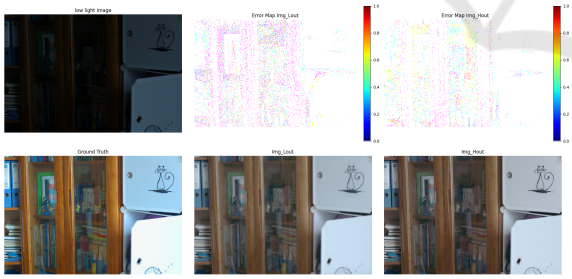

Figure 12: Error Map Analysis for Enhanced Images: The figure illustrates the model's effectiveness in reducing errors. The reduction in error demonstrates the effectiveness of each subnetwork.

5 CONCLUSIONS

In this paper, we introduced GammaWaveletNet (GWNet), a novel approach for low-light image enhancement. GWNet integrates gamma correction, wavelet transforms, and CNN layers within a U-Net architecture. Experimental results demonstrate that GWNet achieves comparable performance to state-of-the-art methods in terms of PSNR and SSIM, while outperforming them in computational efficiency with significantly lower FLOPs and parameter counts. Both visual and quantitative results confirm that GWNet effectively enhances brightness, preserves structural details, and reduces noise, achieving high-quality enhancement.

Future work will focus on optimizing GWNet for mobile devices. This involves reducing computational complexity and memory usage while maintaining performance. By employing hardware acceleration and model compression techniques, we aim to make low-light image enhancement practical for everyday mobile applications.

REFERENCES

Agarap, A. F. (2018). Deep learning using rectified linear units (relu). *arXiv preprint arXiv:1803.08375*.

Banik, P. P., Saha, R., and Kim, K.-D. (2018). Contrast enhancement of low-light image using histogram equalization and illumination adjustment. In *2018 international conference on electronics, information, and Communication (ICEIC)*, pages 1–4. IEEE.

Bhatt, D., Patel, C., Talsania, H., Patel, J., Vaghela, R., Pandya, S., Modi, K., and Ghayvat, H. (2021). Cnn variants for computer vision: History, architecture, application, challenges and future scope. *Electronics*, 10(20):2470.

Brateanu, A., Balmez, R., Avram, A., and Orhei, C. (2024). Lyt-net: Lightweight yuv transformer-based network for low-light image enhancement. *arXiv preprint arXiv:2401.15204*.

Cao, G., Huang, L., Tian, H., Huang, X., Wang, Y., and Zhi, R. (2018). Contrast enhancement of brightness-distorted images by improved adaptive gamma correction. *Computers & Electrical Engineering*, 66:569–582.

Chen Wei, Wenjing Wang, W. Y. J. L. (2018). Deep retinex decomposition for low-light enhancement. In *British Machine Vision Conference*.

Ding, J.-J. (2009). Time frequency analysis and wavelet transform class note. Class notes. Department of Electrical Engineering, National Taiwan University (NTU), Taipei, Taiwan.

Guf, J.-S. and Jiang, W.-S. (1996). The haar wavelets operational matrix of integration. *International Journal of Systems Science*, 27(7):623–628.

Guo, X., Li, Y., and Ling, H. (2016). Lime: Low-light image enhancement via illumination map estimation. *IEEE Transactions on image processing*, 26(2):982–993.

Hai, J., Xuan, Z., Yang, R., Hao, Y., Zou, F., Lin, F., and Han, S. (2023). R2rnet: Low-light image enhancement via real-low to real-normal network. *Journal*

of Visual Communication and Image Representation, 90:103712.

Horé, A. and Ziou, D. (2010). Image quality metrics: Psnr vs. ssim. In *2010 20th International Conference on Pattern Recognition*, pages 2366–2369.

Huang, J., Liu, Y., Zhao, F., Yan, K., Zhang, J., Huang, Y., Zhou, M., and Xiong, Z. (2022). Deep fourier-based exposure correction network with spatial-frequency interaction. In Avidan, S., Brostow, G., Cissé, M., Farinella, G. M., and Hassner, T., editors, *Computer Vision – ECCV 2022*, pages 163–180, Cham. Springer Nature Switzerland.

Huang, S.-C., Cheng, F.-C., and Chiu, Y.-S. (2013). Efficient contrast enhancement using adaptive gamma correction with weighting distribution. *IEEE Transactions on Image Processing*, 22(3):1032–1041.

Hussain, S. A., Chalicham, N., Garine, L., Chunduru, S., Nikitha, V., Prasad V, P., and Sanki, P. K. (2024). Low-light image restoration using a convolutional neural network. *Journal of Electronic Materials*, pages 1–12.

Janocha, K. and Czarnecki, W. M. (2017). On loss functions for deep neural networks in classification. *arXiv preprint arXiv:1702.05659*.

Ji, Z. and Jung, C. (2021). Subband adaptive enhancement of low light images using wavelet-based convolutional neural networks. In *2021 IEEE International Conference on Image Processing (ICIP)*, pages 1669–1673.

Jiang, H., Luo, A., Fan, H., Han, S., and Liu, S. (2023). Low-light image enhancement with wavelet-based diffusion models. *ACM Transactions on Graphics (TOG)*, 42(6):1–14.

Kim, M. W. and Cho, N. I. (2023). Whfl: Wavelet-domain high frequency loss for sketch-to-image translation. In *Proceedings of the IEEE/CVF Winter Conference on applications of computer vision*, pages 744–754.

Mallat, S. (1999). *A Wavelet Tour of Signal Processing*. Electronics & Electrical. Elsevier Science.

Mertens, K. C., Verbeke, L. P., Westra, T., and De Wulf, R. R. (2004). Sub-pixel mapping and sub-pixel sharpening using neural network predicted wavelet coefficients. *Remote Sensing of Environment*, 91(2):225–236.

Nilsson, J. and Akenine-Möller, T. (2020). Understanding ssim. *arXiv preprint arXiv:2006.13846*.

Othman, G. and Zeebaree, D. Q. (2020). The applications of discrete wavelet transform in image processing: A review. *Journal of Soft Computing and Data Mining*, 1(2):31–43.

Rahman, S., Rahman, M. M., Abdullah-Al-Wadud, M., Al-Quaderi, G. D., and Shoyaib, M. (2016). An adaptive gamma correction for image enhancement. *EURASIP Journal on Image and Video Processing*, 2016(1):35.

Ronneberger, O., Fischer, P., and Brox, T. (2015). U-net: Convolutional networks for biomedical image segmentation. In *Medical image computing and computer-assisted intervention–MICCAI 2015: 18th international conference, Munich, Germany, October 5-9, 2015, proceedings, part III 18*, pages 234–241. Springer.

Sakib, S., Ahmed, N., Kabir, A. J., and Ahmed, H. (2019). An overview of convolutional neural network: Its architecture and applications.

Senthilkumar, C. and Kamarasan, M. (2020). An effective classification of citrus fruits diseases using adaptive gamma correction with deep learning model. *Int. J. Eng. Adv. Technol*, 9(2):2249–8958.

Shakibania, H., Raoufi, S., and Khotanlou, H. (2023). Cdan: Convolutional dense attention-guided network for low-light image enhancement.

Ullah, Z., Farooq, M. U., Lee, S.-H., and An, D. (2020). A hybrid image enhancement based brain mri images classification technique. *Medical Hypotheses*, 143:109922.

Wang, C., Wu, H., and Jin, Z. (2023a). Fourllie: Boosting low-light image enhancement by fourier frequency information. In *Proceedings of the 31st ACM International Conference on Multimedia*, pages 7459–7469.

Wang, Q., Wu, B., Zhu, P., Li, P., Zuo, W., and Hu, Q. (2020a). Eca-net: Efficient channel attention for deep convolutional neural networks. In *Proceedings of the IEEE/CVF conference on computer vision and pattern recognition*, pages 11534–11542.

Wang, W., Wu, X., Yuan, X., and Gao, Z. (2020b). An experiment-based review of low-light image enhancement methods. *IEEE Access*, 8:87884–87917.

Wang, Y., Liu, Z., Liu, J., Xu, S., and Liu, S. (2023b). Low-light image enhancement with illumination-aware gamma correction and complete image modelling network. In *Proceedings of the IEEE/CVF International Conference on Computer Vision (ICCV)*, pages 13128–13137.

Wang, Z., Bovik, A., Sheikh, H., and Simoncelli, E. (2004). Image quality assessment: from error visibility to structural similarity. *IEEE Transactions on Image Processing*, 13(4):600–612.

Wang, Z. and Zhang, X. (2024). Contextual recovery network for low-light image enhancement with texture recovery. *Journal of Visual Communication and Image Representation*, 99:104050.

Weeks, M. and Bayoumi, M. (2003). Discrete wavelet transform: architectures, design and performance issues. *Journal of VLSI signal processing systems for signal, image and video technology*, 35:155–178.

Woo, S., Park, J., Lee, J.-Y., and Kweon, I. S. (2018). Cbam: Convolutional block attention module. In *Proceedings of the European conference on computer vision (ECCV)*, pages 3–19.

Xu, B., Wang, N., Chen, T., and Li, M. (2015). Empirical evaluation of rectified activations in convolutional network. *arXiv preprint arXiv:1505.00853*.

Xu, J., Yuan, M., Yan, D.-M., and Wu, T. (2022). Illumination guided attentive wavelet network for low-light image enhancement. *IEEE Transactions on Multimedia*.

Xu, Q., Zhang, R., Zhang, Y., Wang, Y., and Tian, Q. (2021). A fourier-based framework for domain generalization. In *Proceedings of the IEEE/CVF conference on computer vision and pattern recognition*, pages 14383–14392.

Yu, D., Wang, H., Chen, P., and Wei, Z. (2014). Mixed pooling for convolutional neural networks. In *Rough Sets and Knowledge Technology: 9th International Conference, RSKT 2014, Shanghai, China, October 24-26, 2014, Proceedings 9*, pages 364–375. Springer.

Zhang, Z., Zheng, H., Hong, R., Xu, M., Yan, S., and Wang, M. (2022). Deep color consistent network for low-light image enhancement. In *Proceedings of the IEEE/CVF conference on computer vision and pattern recognition*, pages 1899–1908.